

Device variability of Josephson junctions induced by interface roughness

Yu Zhu,¹ Félix Beaudoin,¹ and Hong Guo²

¹⁾*Nanoacademic Technologies Inc., Suite 802, 666 rue Sherbrooke Ouest, Montréal, Québec H3A 1E7, Canada*

²⁾*Department of Physics, McGill University, Montréal, Québec, H3A 2T8, Canada*

(*Electronic mail: eric@nanoacademic.com)

(Dated: 4 February 2026)

As quantum processors scale to large qubit numbers, device-to-device variability emerges as a critical challenge. Superconducting qubits are commonly realized using Al/AlO_x/Al Josephson junctions operating in the tunneling regime, where even minor variations in device geometry can lead to substantial performance fluctuations. In this work, we develop a quantitative model for the variability of the Josephson energy E_J induced by interface roughness at the Al/AlO_x interfaces. The roughness is modeled as a Gaussian random field characterized by two parameters: the root-mean-square roughness amplitude σ and the transverse correlation length ξ . These parameters are extracted from the literature and molecular dynamics simulations. Quantum transport is treated using the Ambegaokar-Baratoff relation combined with a local thickness approximation. Numerical simulations over 5,000 Josephson junctions show that E_J follows a log-normal distribution. The mean value of E_J increases with σ and decreases slightly with ξ , while the variance of E_J increases with both σ and ξ . These results paint a quantitative and intuitive picture of Josephson energy variability induced by surface roughness, with direct relevance for junction design.

I. INTRODUCTION

Superconducting circuits are among the most promising platforms for scalable quantum computing, combining lithographic manufacturability with strong, low-loss nonlinearity from the Josephson effect¹. At the heart of widely used transmon-style devices is an Al/AlO_x/Al Josephson junction shunted by a capacitance, forming a weakly anharmonic quantum oscillator whose lowest two eigenstates $|0\rangle$ and $|1\rangle$ serve as the computational basis². In this picture, the qubit transition frequency is set primarily by the Josephson energy E_J and charging energy E_C , so any process-dependent change in the junction's critical current (and hence E_J) directly shifts the qubit spectrum and operating point. State-of-the-art superconducting quantum processors now contain on the order of 10^2 to 10^3 qubits, exemplified by IBM's 1,121-qubit "Condor" superconducting processor³. However, fault-tolerant quantum computation for societally relevant tasks remains far beyond this scale. For example, detailed resource estimates for Shor's algorithm indicate that factoring a 2048-bit RSA integer would require on the order of tens of millions of noisy physical qubits in a fast-runtime scenario (e.g., ~ 20 million noisy qubits for an 8-hour attack under surface-code assumptions)⁴. This large gap motivates careful attention to device yield and uniformity as superconducting platforms scale toward much larger systems.

Josephson junction variability becomes a central challenge at scale because junctions operate in the tunneling regime, where the critical current I_c depends exponentially on microscopic barrier details; small perturbations—such as local Al/AlO_x thickness fluctuations, effective barrier-height variations, or contamination atoms—can produce significant shifts in E_J , qubit frequency, and gate fidelity. Experimentally, substantial efforts over the past two decades have focused on improving junction reproducibility and understanding microscopic sources of variation, including wafer- and chip-scale resistance/critical-current uniformity studies^{5,6}, process-

optimization of shadow evaporation/oxidation^{6,7}, mitigation strategies for critical-current fluctuations⁸, alternating-bias assisted annealing⁹, and direct microscopy of Al/AlO_x barrier microstructure and thickness distributions^{10,11}. In this work, we focus on variability in E_J induced by Al/AlO_x interface roughness, and present a quantum-mechanical modeling framework that combines quantum transport theory with Gaussian random field models and molecular dynamics simulations to connect microstructural disorder to junction-level Josephson energy statistics.

II. INTERFACE ROUGHNESS MODEL

The rough interface between the aluminum (Al) leads and the aluminum oxide (AlO_x) layer is modeled as a Gaussian random field with a specialized power spectral density. Denote the interface height by $h(x,y)$, where x and y are the transverse coordinates. It is assumed that

$$\langle h(x,y) \rangle = 0, \quad (1)$$

and

$$\langle h(x,y) h(0,0) \rangle = \sigma^2 e^{-\frac{x^2+y^2}{\xi^2}}, \quad (2)$$

where σ is the root-mean-square (RMS) of the interface height along the transport direction, and ξ is the transverse correlation length. Given σ and ξ , a rough interface can be generated by filtering white noise in Fourier space using the corresponding power spectral density, followed by an inverse Fourier transform. Two generated rough interfaces are shown in Fig. 3 (a) and (b).

The transverse correlation length ξ is set by the characteristic lateral length scale of microstructural features in the Al leads—most notably the Al grain size that imprint thickness variations onto the AlO_x barrier. In Al/AlO_x/Al tunnel junction stacks characterized by TEM, the Al electrodes are commonly observed to be polycrystalline with columnar grains on

the order of a few tens of nanometers. For example, Liu *et al.* report crystalline columnar grains of roughly $\sim 20 \text{ nm} \times 30 \text{ nm}$ in qubit Josephson junction electrodes¹¹. A systematic TEM study by Nik *et al.* further shows that the average lateral grain size depends strongly on the Al film thickness: for Al films of 15 nm and 60 nm thickness on oxidized Si, the mean grain size is reported to be on the order of $\sim 38 \text{ nm}$ and $\sim 92 \text{ nm}$, respectively, illustrating that thicker Al films tend to develop larger grains¹². Under other deposition conditions, Fritz *et al.* report that the lower Al layer can exhibit a broad grain size distribution, including grains below $\sim 50 \text{ nm}$, many grains in the $\sim 50 \text{ nm}-150 \text{ nm}$ range, and grains extending up to hundreds of nanometers ($\sim 900 \text{ nm}$) and even $\sim 1 \mu\text{m}$ in lateral size¹¹. These experimental observations suggest choosing ξ to be comparable to the typical lateral grain size for the specific Al growth recipe used in the junction fabrication.

The RMS height σ is set by the vertical amplitude of thickness/height fluctuations, primarily controlled by the Al surface roughness and oxidation/growth nonuniformity. Zeng *et al.* directly measured the local AlO_x thickness in Al/ AlO_x /Al junctions using atomic-resolution STEM and fit the thickness histogram with a Gaussian. They report mean thicknesses 1.66–1.88 nm and standard deviations 0.326–0.372 nm in three samples¹⁰. Fritz *et al.* report AlO_x thickness variation values ranging from 0.29 nm down to 0.11 nm depending on growth conditions¹¹. These experiments suggest a representative range of $\sigma \sim 0.1\text{--}0.3 \text{ nm}$ for high-quality AlO_x tunnel barriers.

Since σ is much smaller than ξ and more difficult to characterize experimentally, we also perform molecular dynamics (MD) simulations to estimate σ . The initial simulation cell contains an Al surface, O_2 molecules, and a vacuum region. In total, the system has 4,380 atoms, comprising 2,880 Al atoms and 750 O_2 molecules, as illustrated in Fig. 1 (a). The Al surface is modeled as an fcc(100) slab consisting of 20 atomic layers, with 144 atoms per layer and a 40 Å vacuum region. The O_2 molecules are placed at random positions with random orientations in a 10 Å thick region between the Al surface and the vacuum. MD simulations are carried out in the NVT ensemble at a fixed temperature 300 K and a fixed volume $34.17 \text{ \AA} \times 34.17 \text{ \AA} \times 78.26 \text{ \AA}$, with periodic boundary conditions in the transverse directions. Interatomic forces and energies are computed using CHGNet, a charge-informed graph-neural-network machine learning interatomic potential pretrained on the Materials Project Trajectory dataset¹³.

MD simulations are performed for 3 ps with a time step of 1 fs. During the first $\sim 2 \text{ ps}$, O_2 molecules react with the Al surface and form an amorphous AlO_x layer with a thickness about 1 nm, as shown in Fig. (b). Then the oxide growth saturates and the remaining O_2 molecules diffuse into the vacuum region. After generating the Al/ AlO_x interface, we remove Al lead atoms and O_2 molecules from the system to expose the AlO_x surface, as shown in Fig. 1 (c). To extract a smooth height profile, we employ a rolling-ball procedure: a probe sphere of radius $R = 3 \text{ \AA}$ is rolled over the AlO_x surface on the Al side to define a continuous surface envelope. The RMS of the surface σ is obtained as 0.97 \AA , 0.76 \AA , 0.81 \AA in three independent MD simulations. We note that σ values extracted

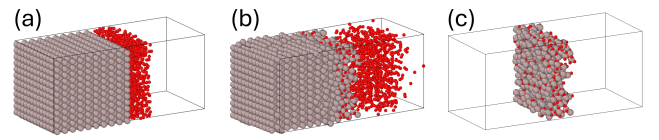


FIG. 1. MD simulation of AlO_x growth. (a) At $t = 0$, fcc(100) Al surface and O_2 molecules. (b) At $t = 3 \text{ ps}$, oxidized Al surface and O_2 molecules. (c) AlO_x layer extracted from (b).

from our MD simulations are smaller than the experimentally reported values. This discrepancy is likely due to the idealized geometry used in the simulations: the Al surfaces are assumed to be atomically flat, whereas real devices typically exhibit additional Al surface roughness that increases the overall height fluctuations.

III. QUANTUM TRANSPORT MODEL

In a Josephson junction, the Josephson energy E_J is related to the critical current I_c by

$$E_J = \frac{\hbar}{2e} I_c, \quad (3)$$

where \hbar is the reduced Planck constant and e is the elementary charge. The critical current can be calculated by solving the Bogoliubov–de Gennes (BdG) equation

$$\begin{pmatrix} H_0(\mathbf{r}) - E_F & \Delta(\mathbf{r}) \\ \Delta^*(\mathbf{r}) & -(H_0(\mathbf{r}) - E_F) \end{pmatrix} \begin{pmatrix} u(\mathbf{r}) \\ v(\mathbf{r}) \end{pmatrix} = E \begin{pmatrix} u(\mathbf{r}) \\ v(\mathbf{r}) \end{pmatrix}, \quad (4)$$

where

$$H_0(\mathbf{r}) = -\frac{\hbar^2}{2m} \nabla^2 + V(\mathbf{r})$$

is the single-particle Hamiltonian, E_F is the Fermi energy, $\Delta(\mathbf{r})$ is the superconducting pair potential, $u(\mathbf{r})$ and $v(\mathbf{r})$ are the electron- and hole-like components of the quasiparticle wavefunction. There are two equivalent theoretical approaches to calculate the supercurrent from the model in Eq. (4). The first approach is the scattering wave function method¹⁴, which provides a clear picture about physical processes such as Andreev reflections and Andreev bound states. The second approach is the Green's function method¹⁵, which offers a unified formalism for general cases and allows effective computational optimization to deal with Andreev bound states¹⁶. However, applying these methods directly to a realistic Josephson junction is not computationally affordable since the size of transport region is as large as $100 \text{ nm} \times 100 \text{ nm} \times 1 \text{ nm}$. The Fermi wavelength of Al, on the other hand, is around 3.6 \AA , estimated using the Fermi energy 11.6 eV. Consequently, the real space resolution should be around 1 \AA , resulting in a $10^3 \times 10^3 \times 10$ real space grid which is too large for numerical simulations.

To tackle the computational challenge, we adopt two approximations to simplify the transport model. The first ap-

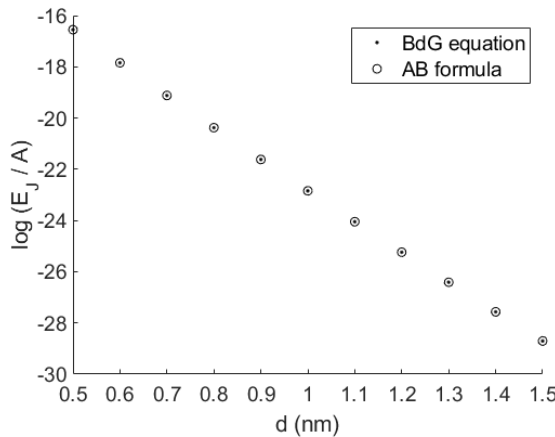


FIG. 2. Josephson energy (log scale) as a function tunnel barrier width, calculated by solving the BdG equation and using the AB relation.

proximation is to use the Ambegaokar–Baratoff (AB) relation

$$I_c = \frac{\pi\Delta}{2eR_N}, \quad (5)$$

which relates the critical current I_c to the normal resistance R_N . The calculation of R_N is much simpler than I_c because it only requires an evaluation of the transmission coefficient at the Fermi energy rather than an integration over the entire energy range. Furthermore, the system size is reduced by half since only the electron-like quasiparticles need to be considered. To assess the accuracy of the AB relation for Josephson junctions, we compare the critical current obtained by solving Eq. (4) with that obtained from the AB relation for a Josephson junction with a square tunnel barrier of height 1.1 eV. As shown in Fig. 2, the results of the two methods agree in high accuracy over a wide range of junction thickness, justifying the use of the AB relation in this study. Moreover, the exponential dependence of E_J on the tunnel barrier thickness d confirms that transport occurs in the tunneling regime.

The second approximation is to separate the transport direction from the transverse directions. Because the junction operates in the tunneling regime, transport is predominantly governed by the local barrier profile along the transport direction, and transverse coupling is negligible. We therefore partition the junction into many independent subsystems in the transverse plane and approximate the total normal conductance as the sum of the conductances of these subsystems. In the continuum limit, this sum becomes an integral of the conductance density over the transverse coordinates. Here, the conductance density is defined as the conductance per unit area for a three-dimensional junction with a uniform cross section in the transverse directions. This local thickness approximation is justified by comparing the relevant length scales of the system. Four characteristic lengths are involved: (1) The Fermi wave length in the Al leads

$$\lambda_F = \frac{2\pi}{k_F} = \frac{2\pi}{\sqrt{\frac{2mE_F}{\hbar^2}}} \approx 3.6 \text{ \AA},$$

where $E_F = 11.6$ eV the Fermi energy of Al bulk. (2) The wave function decaying length in the tunnel barrier

$$\lambda_D = \frac{1}{\kappa} = \frac{1}{\sqrt{\frac{2mU_{\text{barrier}}}{\hbar^2}}} = 1.9 \text{ \AA},$$

where $U_{\text{barrier}} = 1.1$ eV is the effective tunnel barrier height of the Al/AlO_x interface. (3) The RMS of interface roughness along the transport direction: $\sigma \sim 0.1$ nm. (4) The correlation length of interface roughness in the transverse directions: $\xi \sim 10$ nm. The change of the tunnel barrier thickness over a lateral distance λ_F is estimated as $\frac{\lambda_F}{\xi} \sigma$. Since

$$\frac{\lambda_F}{\xi} \sigma \ll \lambda_D.$$

the tunnel barrier can be viewed as an ensemble of locally uniform tunnel barriers, which justifies the local thickness approximation.

IV. RESULTS

The interface roughness model and quantum transport framework are combined to study the variability of the Josephson energy E_J in Al/AlO_x/Al junctions. The junction is modeled as two free-electron metallic leads separated by a three-dimensional tunnel barrier. The tunnel barrier is characterized by a height $U \sim 1$ eV, a width $d \sim 1$ nm, and a cross section $L_x \times L_y = 200$ nm \times 200 nm, consistent with Al/AlO_x interface. The leads are characterized by a Fermi energy $E_F = 11.7$ eV and a superconducting gap $\Delta = 0.2$ meV, consistent with bulk Al. The interface roughness between the two leads and the tunnel barrier is described by the Gaussian random field model in Eqs. (1,2) with parameters RMS amplitude σ and transverse correlation length ξ . For simplicity, it is assumed that σ and ξ are identical for the two Al/AlO_x interfaces in the Josephson junction. The resulting local barrier thickness is obtained by adding the two interfacial height profiles to the nominal thickness d , thus defining the spatially varying tunnel-barrier profile used in the transport calculation.

To be more specific, let us choose the tunnel barrier parameters as $d = 1.0$ nm and $U = 1.1$ eV, and set the interface roughness parameters as $\sigma = 0.85$ \AA and $\xi = 10$ nm. Fig. 3 (a) and (b) are the colormaps of the resulting interface roughness, showing fluctuations at the scale of transverse correlation length ξ . Fig. 3 (c) is the normalized histogram of the calculated E_J over 5,000 Josephson junctions with different tunnel barrier profiles. It is very interesting that the distribution of E_J is not a Gaussian but skewed toward larger values. This feature can be understood as a result of the tunneling physics. Suppose the effective tunnel barrier width is normally distributed and since E_J has an exponential dependence on the tunnel barrier width, the distribution of E_J must follow a log-normal distribution, and the corresponding probability density function is

$$p(E_J > 0) = \frac{1}{E_J \sigma_J \sqrt{2\pi}} \exp \left[-\frac{(\log E_J - \mu_J)^2}{2\sigma_J^2} \right], \quad (6)$$

where μ_J and σ_J are the mean and standard deviation of E_J . Consequently, the mean and variance of E_J are

$$\mathbb{E}[E_J] = e^{\mu_J + \sigma_J^2/2},$$

and

$$\text{Var}(E_J) = (e^{\sigma_J^2} - 1) e^{2\mu_J + \sigma_J^2},$$

respectively. These expressions show why the distribution of E_J over the ensemble of the Josephson junctions becomes increasingly skewed and broadened as the underlying fluctuations grow. Fitting the histogram with Eq. (6), we obtain

$$E_J/h = 20.447 \pm 2.326 \text{ GHz}. \quad (7)$$

For transmons, the qubit transition frequency is determined by E_C and E_J as²

$$\frac{\omega_{01}}{2\pi} = \frac{1}{h}(E_1 - E_0) \approx \frac{1}{h}(\sqrt{8E_C E_J} - E_C).$$

Therefore, the standard deviation of $\frac{\omega_{01}}{2\pi}$ is related to that of E_J by

$$\Delta \frac{\omega_{01}}{2\pi} = \frac{1}{h} \sqrt{\frac{2E_C}{E_J}} \Delta E_J.$$

Using the mean and standard deviation of E_J in Eq. (7) and assuming $E_C/h = 0.25$ GHz, we obtain the mean and standard deviation of $\omega_{01}/2\pi$ as

$$\omega_{01}/2\pi = 6.145 \pm 0.364 \text{ GHz}. \quad (8)$$

Next, we investigate the dependence of the E_J variability on the roughness parameters σ and ξ . Table I lists the calculated mean and standard deviation of E_J as functions of σ and ξ , while fixing the other device parameters at $U = 1.1$ eV, $d = 1.0$ nm, $\Delta = 0.2$ meV, $E_F = 11.7$ eV. Two main trends are observed. (1) With increasing σ , both $\mathbb{E}[E_J]$ and $\text{Var}(E_J)$ increase. $\text{Var}(E_J)$ increases because the amplitude of thickness fluctuations scales with σ , leading to stronger sample-to-sample variations in E_J . The rise in $\mathbb{E}[E_J]$ reflects the exponential sensitivity of tunneling to the local barrier thickness: the total conductance is dominated by rare, anomalously thin regions, which become thinner and more influential as σ grows. (2) With increasing ξ , $\mathbb{E}[E_J]$ decreases slightly, whereas $\text{Var}(E_J)$ increases markedly, and both trends saturate once ξ becomes comparable to the lateral size of the junction. The increase of $\text{Var}(E_J)$ can be understood as a consequence of reduced self-averaging. The junction may be viewed as comprising many parallel tunneling channels, each characterized by a correlation area of order ξ^2 . A larger ξ implies fewer statistically independent channels, which in turn leads to enhanced sample-to-sample fluctuations and a larger variance. Meanwhile, the slight decrease of $\mathbb{E}[E_J]$ is associated with finite-size effect. For a junction with a finite cross section, increasing ξ reduces the number of independent segments across the interface. Consequently, the probability of

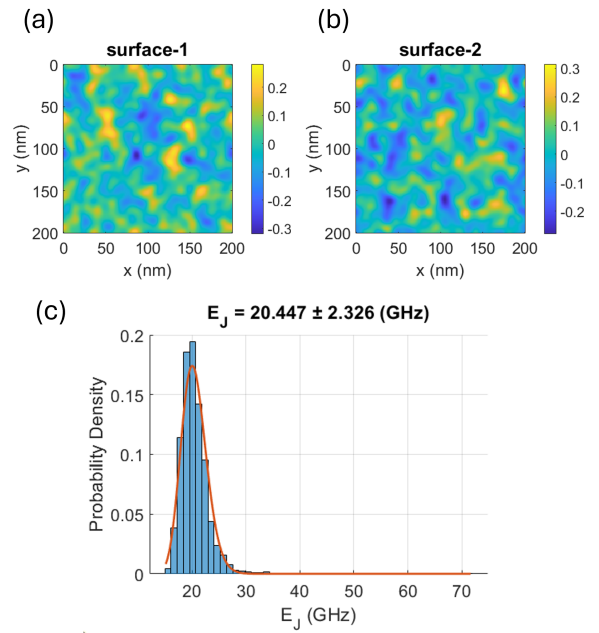


FIG. 3. (a) and (b): Colormaps of Al/AlO_x interface roughness. (c): Histogram of E_J over 5,000 Josephson junctions. The orange line is a fit to Eq. 6.

TABLE I. Josephson energy E_J/h (GHz) as a function of RMS roughness σ and transverse correlation length ξ . Values are given as mean \pm standard deviation.

ξ (nm)	$\sigma = 0.08$ nm	$\sigma = 0.09$ nm	$\sigma = 0.10$ nm
10	17.92 ± 1.70	23.57 ± 3.20	32.32 ± 6.15
20	17.86 ± 3.05	23.39 ± 5.45	31.81 ± 9.82
30	17.72 ± 3.99	23.05 ± 6.87	31.06 ± 11.94
40	17.54 ± 4.70	22.67 ± 7.89	30.27 ± 13.35
50	17.37 ± 5.24	22.32 ± 8.64	29.56 ± 14.35

realizing rare, exceptionally thin barrier regions that would otherwise dominate the tunneling contribution is reduced, resulting in a modest suppression of $\mathbb{E}[E_J]$. When ξ approaches the junction dimension, the effective number of independent segments becomes $O(1)$, and both the mean and variance of E_J become insensitive to further increases in ξ , resulting in saturation behavior.

V. SUMMARY

To summarize, we have investigated the variability of the Josephson energy E_J in Al/AlO_x/Al junctions arising from interface roughness. The roughness is modeled using a Gaussian random field characterized by the RMS amplitude σ and the transverse correlation length ξ . The values of these parameters are taken from the experimental literature and extracted from our atomistic MD simulations. The quantum transport model is based on the Ambegaokar-Baratoff rela-

tion combined with a local thickness approximation, both of which are justified and numerically verified for the Josephson junctions. Numerical simulations over an ensemble of 5,000 samples show that E_J follows a log-normal distribution. The mean value of E_J increases with σ and decreases slightly with ξ , while the variance of E_J increases with both σ and ξ . In this work, we have assumed that σ and ξ are independent structural parameters and are identical for the two interfaces in Al/AlO_x/Al junctions. While reasonable, these assumptions require careful experimental verification under different growth and process conditions. Connecting our model to the experimental characterization of the fabricated Josephson junctions and combining the superconductivity solvers employed here with computational microwave engineering software¹⁷ will be important directions for future work, opening the door to the co-design of Josephson junctions and their neighboring superconducting-circuit elements.

VI. ACKNOWLEDGEMENTS

We thank the Digital Research Alliance of Canada for the computational facilities that made this work possible. H.G. is grateful to NSERC of Canada for partial financial support. The authors thank Drs. Raphaël Prentki, Pericles Philipopoulos, and Igor Benek-Lins for useful discussions regarding the interface roughness model, the transmon and the superconducting qubits.

- ¹M. H. Devoret and R. J. Schoelkopf, “Superconducting circuits for quantum information: an outlook,” *Science* **339**, 1169–1174 (2013).
- ²J. Koch, T. M. Yu, J. Gambetta, A. A. Houck, D. I. Schuster, J. Majer, A. Blais, M. H. Devoret, S. M. Girvin, and R. J. Schoelkopf, “Charge-insensitive qubit design derived from the cooper pair box,” *Physical Review A* **76**, 042319 (2007).
- ³J. Gambetta, “The hardware and software for the era of quantum utility is here,” (2023).
- ⁴C. Gidney and M. Ekerå, “How to factor 2048 bit RSA integers in 8 hours using 20 million noisy qubits,” *Quantum* **5**, 433 (2021), 1905.09749.
- ⁵J. M. Kreikebaum, K. P. O’Brien, A. Morvan, and I. Siddiqi, “Improving wafer-scale Josephson junction resistance variation in superconducting quantum coherent circuits,” *Superconductor Science and Technology* **33**, 06LT02 (2020), 1909.09165.
- ⁶A. A. Pishchimova, N. S. Smirnov, D. A. Ezenkova, E. A. Krivko, E. V. Zikiy, D. O. Moskalev, A. I. Ivanov, N. D. Korshakov, and I. A. Rodionov, “Improving josephson junction reproducibility for superconducting quantum circuits: junction area fluctuation,” *Scientific Reports* **13**, 6772 (2023), 10.1038/s41598-023-34051-9.
- ⁷D. O. Moskalev, E. V. Zikiy, A. A. Pishchimova, D. A. Ezenkova, N. S. Smirnov, A. I. Ivanov, N. D. Korshakov, and I. A. Rodionov, “Optimization of shadow evaporation and oxidation for reproducible quantum josephson junction circuits,” *Scientific Reports* **13**, 4174 (2023), 10.1038/s41598-023-31003-1.
- ⁸S. Song, Y. Sun, J. Xu, Z. Han, X. Yang, X. Wang, S. Li, D. Lan, J. Zhao, X. Tan, and Y. Yu, “Mitigation of critical current fluctuation of josephson junctions in superconducting quantum circuits,” *Applied Physics Letters* **118**, 244004 (2021), 10.1063/5.0049637.
- ⁹D. P. Pappas, M. Field, C. J. Kopas, J. A. Howard, X. Wang, E. Lachman, J. Oh, L. Zhou, A. Gold, G. M. Stiehl, *et al.*, “Alternating-bias assisted annealing of amorphous oxide tunnel junctions,” *Communications Materials* **5**, 150 (2024).
- ¹⁰L. J. Zeng, S. Nik, T. Greibe, C. M. Wilson, P. Delsing, and E. Olsson, “Direct observation of the thickness distribution of ultra thin AlO_x barrier in Al/AlO_x/Al Josephson junctions,” *Journal of Physics D: Applied Physics* **48**, 395308 (2015), 1407.0173.
- ¹¹S. Fritz, L. Radtke, R. Schneider, M. Weides, and D. Gerthsen, “Optimization of Al/AlO_x/Al-layer systems for Josephson junctions from a microstructure point of view,” *Journal of Applied Physics* **125**, 165301 (2019), 1901.09625.
- ¹²S. Nik, P. Krantz, L. Zeng, T. Greibe, H. Pettersson, S. Gustafsson, P. Delsing, and E. Olsson, “Correlation between Al grain size, grain boundary grooves and local variations in oxide barrier thickness of Al/AlO_x/Al tunnel junctions by transmission electron microscopy,” *SpringerPlus* **5**, 1067 (2016).
- ¹³B. Deng, P. Zhong, K. Jun, J. Riebesell, K. Han, C. J. Bartel, and G. Ceder, “Chgnet as a pretrained universal neural network potential for charge-informed atomistic modelling,” *Nature Machine Intelligence* **5**, 1031–1041 (2023).
- ¹⁴G. E. Blonder, M. Tinkham, and T. M. Klapwijk, “Transition from metallic to tunneling regimes in superconducting microconstrictions: Excess current, charge imbalance, and supercurrent conversion,” *Physical Review B* **25**, 4515–4532 (1982).
- ¹⁵Q. F. Sun, B. Wang, J. Wang, and T. H. Lin, “Electron transport through a mesoscopic hybrid multiterminal resonant-tunneling system,” *Physical Review B* **61**, 4754–4761 (2000).
- ¹⁶Y. Zhu, Q. Sun, and T. Lin, “Probing spin states of coupled quantum dots by a dc josephson current,” *Physical Review B* **66**, 085306 (2002).
- ¹⁷Nanoacademic Technologies Inc., “QTCAD: Superconductors – Theory,” https://docs.nanoacademic.com/qtcad/theory_sc/theory_sc/ (2026).
- ¹⁸L. Zeng, D. T. Tran, C.-W. Tai, G. Svensson, and E. Olsson, “Atomic structure and oxygen deficiency of the ultrathin aluminium oxide barrier in Al/AlO_x/Al Josephson junctions,” *Scientific Reports* **6**, 29679 (2016).
- ¹⁹X. Liu, K. Pan, Z. Zhang, and Z. Feng, “Unveiling atomic structure and chemical composition of the al/alox/al josephson junctions in qubits,” *Applied Surface Science* **640**, 158337 (2023).